

Probing the local rapidity distribution of a 1D Bose gas

L. Dubois,¹ G. Thémèze,¹ F. Nogrette,¹ J. Dubail,² and I. Bouchoule¹

¹*Laboratoire Charles Fabry, Institut d'Optique Graduate School,
CNRS, Université Paris-Saclay, 91127 Palaiseau, France*

²*LPCT, CNRS & Université de Lorraine, UMR 7019, 54000 Nancy, France*

One-dimensional Bose gases with contact repulsive interactions are characterized by the presence of infinite-lifetime quasiparticles whose momenta are called the ‘rapidities’. Here we develop a probe of the local rapidity distribution, based on the fact that rapidities are the asymptotic momenta of the particles after a very long one-dimensional expansion. This is done by performing an expansion of a selected slice of the gas. As a proof of concept, we apply this to a cloud at equilibrium in a trap. While for realistic expansion times the asymptotic regime is barely reached, we show that the expansion dynamics follows the hydrodynamic scaling such that one can use the theory of Generalized Hydrodynamics to analyze the expansion. Our data are in good agreement with the theory.

Ultracold atomic gases have long been identified as versatile platforms for the investigation of quantum many-body physics [1, 2]. In particular, freezing out degrees of freedom, it is possible to experimentally realize various paradigmatic models of low-dimensional many-body physics, such as one-dimensional (1D) gases with contact interactions [3–9]. The latter include gases of bosons [4–6, 8, 10, 11], fermions [7, 9, 12], sometimes with multiple components [12–14]. Those systems, benchmarked successfully against theoretical predictions at equilibrium [10, 11, 15–17], have led to many fundamental advances on out-of-equilibrium quantum many-body dynamics [8, 18–23].

The single-component 1D gas of bosons with contact repulsive interactions is the simplest of all 1D gases. It is a key example of an integrable quantum-many body system [24, 25], first investigated theoretically by Lieb and Liniger [26, 27]. The key notion in the theory is the distribution of rapidities, which can be understood in at least three different ways. A first — intuitive — way of thinking of the rapidities is as the velocities of infinitely long-lived quasi-particles that travel through the system (see e.g. [28–30]). A second — more formal — perspective is to view the rapidities as parameters of the energy eigenstates, which take the form of a Bethe wavefunction [24–27]: $\psi(x_1, x_2, \dots, x_N) \propto \sum_{\sigma} \mathcal{A}_{\sigma}(\theta_1, \dots, \theta_N) \prod_{j=1}^N e^{imx_j \theta_{\sigma(j)}/\hbar}$ for an eigenstate of energy $E = \sum_{j=1}^N m\theta_j^2/2$, where m is the atom mass. Here the sum runs over all permutations σ of N indices, the x_j ’s are the positions of the atoms, and the \mathcal{A}_{σ} ’s are amplitudes whose calculation is a key step in diagonalizing the Hamiltonian by Bethe Ansatz [24–27]. Finally, a third perspective — a more operational one — consists in viewing the rapidities as the *asymptotic velocities of the atoms* after a 1D free expansion [31–33]: after a long 1D expansion time τ , such that the interactions have become negligible, the atoms are located at positions $x_j \simeq \theta_j \tau$ [32, 33] and their velocity is θ_j .

The latter operational perspective is particularly relevant for experiments, as it allows to measure the global rapidity distribution of an experimental system, by per-

forming a 1D expansion before measuring either the density profile or the momentum distribution of all the atoms. The first such measurements were performed very recently in bundles of 1D gases trapped in a 2D optical array [22], see also subsequent works [34–36].

We stress that, in these recent experimental achievements, it is always the *global rapidity distribution* that is measured: it is the rapidity distribution of a whole 1D atom cloud regardless of its inhomogeneity — moreover, because the measurement is performed on a bundle of 1D tubes, the distribution is also averaged over all the tubes—. In contrast, in this Letter, our goal is to experimentally probe the *local rapidity distribution* of a single inhomogeneous 1D Bose gas. We develop an experimental protocol for this, and, as a proof of concept, we report experimental results for a 1D Bose gas at equilibrium in a harmonic potential.

The notion of *local rapidity distribution* naturally arises when one considers inhomogeneous atom clouds at equilibrium in a slowly varying potential, within the Local Density Approximation (LDA) [10, 16, 37]. In that approach the gas is viewed as a continuous fluid, where each point is a fluid cell assumed to be in a thermodynamic macrostate. In integrable 1D gases, the thermodynamic macrostates are Generalized Gibbs Ensembles [38–42] parameterized by their intensive rapidity distribution $\rho(\theta)$ — which, in a fluid cell of length ℓ containing particles with rapidities θ_j , $j = 1, \dots, N_{\ell}$, corresponds to $\rho(\theta) = \frac{1}{\ell} \sum_{j=1}^{N_{\ell}} \delta(\theta - \theta_j)$ — [39, 43]. The continuous description of these gases within LDA involves one such distribution $\rho(\theta)$ for each fluid cell at point x : this is the *local rapidity distribution* $\rho(x, \theta)$.

Note that the local rapidity distribution plays a key role, not only in equilibrium, but also in the out-of-equilibrium dynamics of the gas, provided the latter is sufficiently slow to ensure local relaxation to macrostates. The time-evolution of $\rho(x, \theta)$ is precisely the topic of Generalized Hydrodynamic (GHD) [28, 44], a theory which has attracted much attention lately, see e.g. [33, 45–51].

To experimentally probe the *local rapidity distribution* we propose the following protocol. With a laser beam,

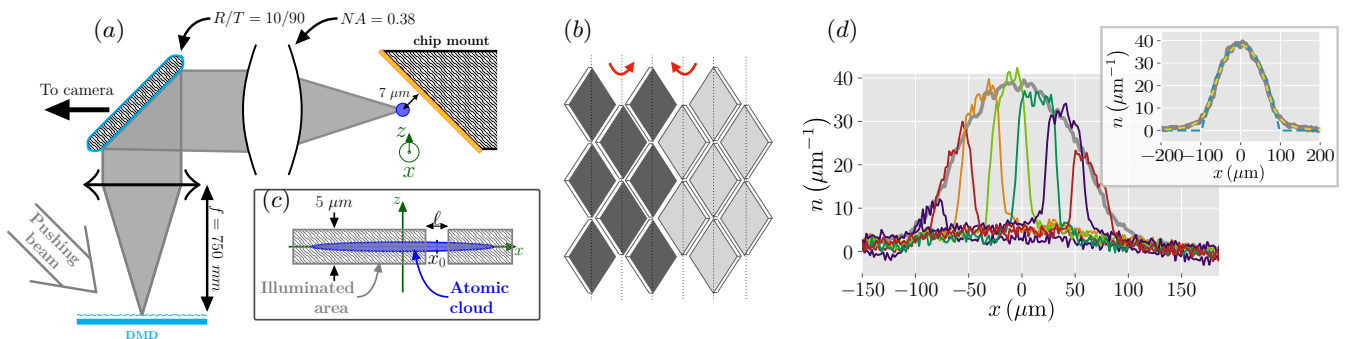


Figure 1. Selection of a ‘slice’ of the 1D cloud. (a) The atoms are trapped $7 \mu\text{m}$ under the atom chip, which is covered by a gold mirror. The pushing beam reflects on a micro-mirror matrix (DMD), which is optically conjugated with the plane (x, z) containing the atomic cloud. The optical system includes a R:T=10:90 plate such that it contains the objective of numerical aperture 0.38, used also for absorption images. (b) Each micro-mirror is tilted by ± 12 degree, such that it either sends the beam towards the imaging system (grey micro-mirrors) or deviates it away. (c) Pushing beam intensity in the plane of the atoms: grey area are the illuminated zones. (d) In situ density profiles measured after slicing at different positions x_0 . In the background we show the density profile of the initial cloud, before the slicing. Inset: the density profile before slicing is well fitted by the theory prediction at thermal equilibrium at temperature $T_{YY} = 90 \text{ nK}$ and chemical potential $\mu_{YY} = 49 \text{ nK} \times k_B$ (dashed yellow line). The parabolic profile expected for the quasi-condensate equation-of-state is also shown (blue dashed line).

one can ‘slice’ the 1D atom cloud (Fig. 1): by radiation pressure it is possible to almost instantaneously remove all the atoms outside a selected interval $[x_0 - \ell/2, x_0 + \ell/2]$, leaving only the atoms inside the ‘slice’ of length ℓ unaffected. The atoms in the slice are in a macrostate characterized by the rapidity distribution $\int_{x_0 - \ell/2}^{x_0 + \ell/2} \rho(x, \theta) dx / \ell \simeq \rho(x_0, \theta)$. Then, by letting the atoms in the slice expand along the 1D waveguide, and by measuring the atom density $n(x, \tau)$ after a long expansion time τ (Fig. 3), one can access the rapidity distribution

$$\rho(x_0, \theta) \simeq \tau n(x_0 + \theta\tau, \tau) / \ell. \quad (1)$$

This method gives access to $\rho(x_0, \theta)$ with a finite resolution $\Delta v \sim \hbar / (m\ell)$, and our slices are always very long, so that $\Delta\theta$ is always much smaller than the typical width of our rapidity distributions. Repeating the same procedure for slices centered on different positions x_0 allows to map out the distribution in the whole (x, θ) -plane.

In this Letter, we implement this protocol for a gas at equilibrium in a harmonic potential (Fig. 2). The results are in good agreement with the theory expectation for a local rapidity distribution $\rho(x, \theta)$ at thermal equilibrium in the trap, despite limitations discussed in detail below. We now turn to a full description of the experimental protocol and benchmarks.

Atom chip setup. Our 1D clouds are obtained by trapping ^{87}Rb atoms in the $|F=2, m_F=2\rangle$ state in a magnetic field created by currents running through microwires on a chip [52]. The transverse trapping potential, which confines the atoms in 1D, is created by three parallel 1 mm-long microwires [53], with currents modulated at 400 KHz. The atoms are guided $15 \mu\text{m}$ above the central wire ($7 \mu\text{m}$ above the golden mirror that covers the chip), in a transverse potential that is quasi-harmonic with frequency $\omega_{\perp} / 2\pi = 2.6 \text{ KHz}$. For atoms in the

transverse ground state, the effective 1D coupling constant is $g = 2a_{3D}\hbar\omega_{\perp}$ [54], where $a_{3D} = 5.3 \text{ nm}$ is the 3D scattering length of ^{87}Rb [55]. A longitudinal potential $V(x) = m\omega^2 x^2 / 2$ with $\omega / 2\pi = 5.0 \text{ Hz}$ is created independently by perpendicular wires with continuous current. This setup ensures independent control of the transverse and longitudinal potentials, a crucial point for measuring the rapidities, as one needs to perform 1D expansions by switching off the potential $V(x)$ while maintaining the transverse confinement.

All data are extracted from absorption images. Prior to the absorption pulse, all confinements are removed and the cloud undergoes a 1 ms time of flight, long enough to remove the effects of strong atomic densities on absorption but short enough to leave the longitudinal density profile unaffected. The latter is obtained by integrating the absorption images transversally.

Our cold atom clouds at equilibrium are prepared using radiofrequency forced evaporation. They typically contain $N \simeq 5 \times 10^3$ atoms. The experimental atom density $n(x)$ is accurately fitted by the LDA prediction based on the Yang-Yang equation of state at thermal equilibrium [10, 16, 33] (Fig. 1(c), inset). The temperature and chemical potential estimated from the fit, $T_{YY} = 90 \text{ nK}$ and $\mu_{YY} / k_B = 49 \text{ nK}$, are smaller than $\hbar\omega_{\perp} / k_B = 123 \text{ nK}$, such that one expects the 1D analysis to hold. To further estimate the occupation of transverse excited states, we have fitted the atom density using the modified Yang-Yang equation state of Ref. [10]; we find a negligible improvement corresponding to a local fraction of transversally excited atoms that never exceeds 6%. This confirms that our clouds are well in the 1D regime.

The gas is weakly interacting, with a dimensionless repulsion strength at the center of the trap $\gamma =$

$mg/(\hbar^2 n(0)) \simeq 0.7 \times 10^{-2}$, and the temperature of our 1D clouds satisfies $k_B T \ll n(0)^{3/2} \sqrt{\hbar^2 g/m}$ (see [15] or Eq. (66) in [33]), implying that the gas is in the quasi-condensate regime near the trap center. There, the equation of state is close to that of a Bose-Einstein condensate, $\mu \simeq gn$, leading to an LDA density profile $n(x) \simeq (\mu - V(x))/g$ near the trap center (Fig. 1(c), inset).

Slicing the cloud. To cut a slice $[x_0 - \ell/2, x_0 + \ell/2]$ of the cloud, we shine the atoms out of the selected interval with a beam perpendicular to the x -axis (Fig. 1(a)), at a frequency close to the $F = 2 \rightarrow F' = 3$ cycling hyperfine transition of the D2 line. After about 15 absorption-spontaneous emission cycles, the atoms are no longer confined in 1D, either because they fall in an untrapped Zeeman state, or because their kinetic energy exceeds the trap depth. In order to spatially shape the pushing beam so that the zone $[x_0 - \ell/2, x_0 + \ell/2]$ stays in the dark, we use a digital micro-mirror device (DMD) that is imaged on the atoms (Fig. 1(b,c)) through a high numerical aperture objective. We apply a $30 \mu\text{s}$ beam pulse, with an intensity adjusted so that more than 99% of the atoms are removed. The photon scattering rate is smaller than the natural linewidth so that scattered photons are mainly emitted at the laser frequency, and we detune the laser by 15 MHz in order to mitigate reabsorption of the scattered photons by atoms in the dark zone.

In Fig. 1(c) we show the atom density $n(x)$ measured before slicing (gray line) and after slicing (colored lines), for slices centered on seven different positions x_0 . The slice width is $\ell = 37 \mu\text{m}$. Each profile is averaged over 30 shots. The delay between the pushing beam and the imaging beam is only 1.1 ms such that some of the pushed atoms, although they are no longer trapped, are still in the vicinity of the 1D cloud. These atoms contribute to the absorption, which explains the background seen in Fig. 1(c). Even for the smallest slice width we tested, $\ell = 25 \mu\text{m}$, the number of atoms that remain trapped after the slicing is equal, within measurement precision, to its expected value $\ell n(x_0)$.

Profiles after expansion of $\tau = 40$ ms. Right after the pushing pulse, the longitudinal confinement is switched off, and the cloud expands along the 1D waveguide. We measure the density profile $n(x)$ after an expansion time $\tau = 40$ ms. In Fig. 2(a) we show the rescaled profiles $\tau n(x, \tau)/\ell$ after expansion, for the seven different slices of Fig. 1(c) centered on different positions x_0 . For each slice, we plot the rescaled profile as a function of the ‘rapidity’ $\theta = (x - x_0)/\tau$. This gives an estimate of the rapidity distribution in the whole (x, θ) -plane, following Eq. (1). For comparison, in Fig. 2(b) we show the theoretical rapidity distribution $\rho(x, \theta)$ for the thermal equilibrium in the harmonic potential $V(x)$ at the temperature T_{YY} and chemical potential μ_{YY} obtained fitting the density profile. We find a good agreement between the experimental measurement and the theory expectation. However, this comparison assumes that the expansion time is large enough so that the density pro-

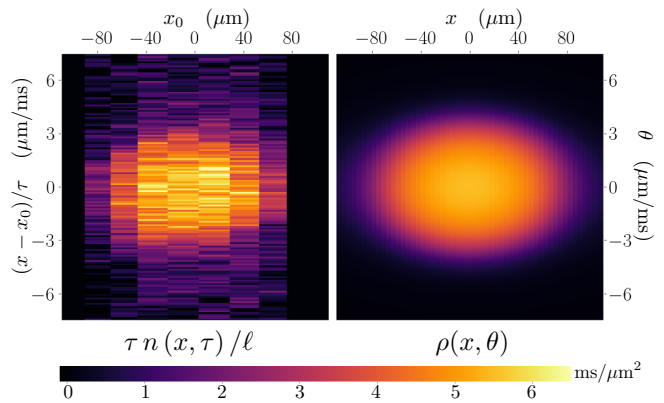


Figure 2. (a) Rescaled density profiles $\tau n/\ell$ with $\tau = 40$ ms and $\ell = 37 \mu\text{m}$ for the different slices of Fig. 1(c), centered on different positions x_0 . (b) Theory prediction for the rapidity distribution $\rho(x, \theta)$ at thermal equilibrium in the potential $V(x)$ at the temperature T_{YY} and chemical potential μ_{YY} (obtained by fitting the in situ profile in Fig. 1(d)).

file has converged to the rapidity distribution. To test this assumption, we turn to an analysis of the expansion dynamics.

Hydrodynamic scaling of slice expansion. We start by checking that our measured expansion profiles are independent of the slice length ℓ when one rescales the position and expansion time,

$$n(x, \tau) = \mathcal{G}[\rho_0]((x - x_0)/\ell, \tau/\ell) \quad (2)$$

for some function \mathcal{G} that depends on the initial rapidity distribution ρ_0 in the slice, which is assumed to be uniform. Such scaling must hold for any inviscid fluid whose description by hydrodynamic equations includes no dissipative terms (or spatial derivatives of higher order) —this is also known as the ‘Euler scale’ or ‘hydrodynamic limit’ [56]—. This ‘Euler’ scaling is well satisfied by our expansion data, at least for slices near the center of the cloud (Fig. 3(a)). In fact, comparing data sets with different initial densities $n_0 = n(x_0, 0)$, we find that our profiles are approximately compatible with a stronger scaling relation (Fig. 3(b)),

$$n(x, \tau) \simeq n_0 \times \mathcal{F}\left(\frac{x - x_0}{\ell}, \sqrt{\frac{gn_0}{m}} \frac{\tau}{\ell}\right), \quad (3)$$

for some dimensionless function \mathcal{F} . This scaling is expected to hold for a gas deep in the quasi-condensate regime —such as our clouds near the trap center—. Indeed, this is a straightforward consequence of Gross-Pitaevskii (GP) hydrodynamic equations $\partial_t n + \partial_x(vn) = 0$, $\partial_t v + v\partial_x v = -g\partial_x n$, which are valid in that regime. The analytical expression of \mathcal{F} is unknown to our knowledge, besides its asymptotic value: since the ground state rapidity distribution in that regime is $\rho(\theta) \simeq m\sqrt{4gn_0/m - \theta^2}/(2\pi g)$ [26, 27], we expect from Eq. (1) that $\mathcal{F}(\alpha, \beta) \simeq \sqrt{4 - (\alpha/\beta)^2}/(2\pi\beta)$ for large β . The

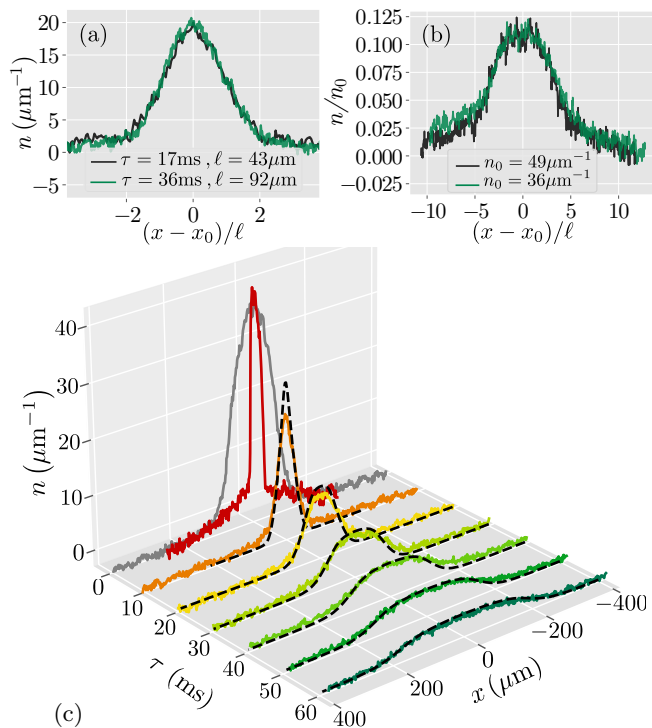


Figure 3. (a) ‘Euler’ scaling (Eq. (2)). For a fixed value $\tau/\ell = 0.39$ ms/ μm , we compare the density profiles for slices with different ℓ centered on $x_0 = 0$. (b) GP hydrodynamic scaling (Eq. (3)): for a given $\sqrt{gn_0/m} \times \tau/\ell = 2.65$, and for $\ell = 37\mu\text{m}$, we plot the density profiles for two different densities n_0 , obtained by slicing the cloud at different position x_0 . (c) 1D expansion of the slice at $x_0 = 0$ of width $\ell = 37\mu\text{m}$. The grey profile corresponds to the initial cloud. The density profiles after different expansion times are plotted in colored lines. Black dashed lines are GHD calculations done for an initial thermal rapidity distribution at the temperature T_{YY} and chemical potential $\mu(x_0) = \mu(0) = \mu_{\text{YY}}$, where T_{YY} and μ_{YY} are extracted from the in situ profile (Fig. 1(d)).

rapidity distribution near the center of the cloud is expected to be close to this semi-circle distribution, as seen in Fig. 4 which compares it to the thermal rapidity distribution at T_{YY} and μ_{YY} .

Comparison of the observed expansion with GHD calculations. Since our data fulfills the Euler hydrodynamic scaling (2), we expect the expansion to be well modeled by GHD [28, 44]. GHD coincides with GP hydrodynamics —as long as the latter does not develop shocks— at zero temperature and in the regime of weak repulsion [57–59], but it is much more general and it applies to all interaction regimes and to finite entropy situations [33]. In particular, here, it naturally incorporates all deviations from GP hydrodynamics caused by departure from the weakly interacting regime or by the fact the initial state differs from the ground state. The rapidity distribution $f(x, \theta, \tau)$, initially equal to $f(x, \theta, 0) = \rho(x_0, \theta)$ if $|x - x_0| \leq \ell/2$ and $f(x, \theta, 0) = 0$

otherwise, evolves according to

$$\partial_\tau f + \partial_x (v_{[f]}^{\text{eff}} f) = 0, \quad (4)$$

where the effective velocity satisfies the integral equation $v_{[f]}^{\text{eff}}(\theta) = \theta - \int \frac{2g/m}{g^2/\hbar^2 + (\theta - \theta')^2} [v_{[f]}^{\text{eff}}(\theta) - v_{[f]}^{\text{eff}}(\theta')] f(\theta') d\theta'$. GHD is an ‘Euler-scale’ hydrodynamic theory, so the solution of Eq. (4) is a function of $(x - x_0)/\ell$ and τ/ℓ as we have seen. In Fig. 3(c) we compare our experimental expansion profiles for the central slice to the results of the GHD simulation, assuming that the rapidity distribution is that of a thermal state at the temperature T_{YY} and the chemical potential μ_{YY} obtained by fitting the equilibrium profile (Fig. 1(d)). For a more detailed comparison, in Fig. 4 we plot the profiles at 50 ms expansion time. We find a good agreement between data and calculations, confirming that GHD captures the expansion dynamics.

We can then use GHD simulations to investigate the convergence of the expansion profiles towards the rapidity distribution. The inset of Fig. 4 compares the GHD density profile after 50 ms of expansion to its asymptotic form given by Eq. (1). We find deviations by about 12% in the central part. A convergence to better than 2% would require an unrealistic expansion time of 400 ms. Thus, using Eq. (1) to deduce the rapidity distribution from the profiles after expansion gives only an approximate estimate of the rapidity distribution. Nevertheless, for each x_0 , one could in principle extract $\rho(x_0, \theta)$ from a fit of the measured density profile after expansion with the one calculated with GHD. For this, one needs an ansatz for the initial state $\rho(x_0, \theta)$, parameterized by a few parameters, whose number are limited by the finite signal over noise of the data and the calculation time.

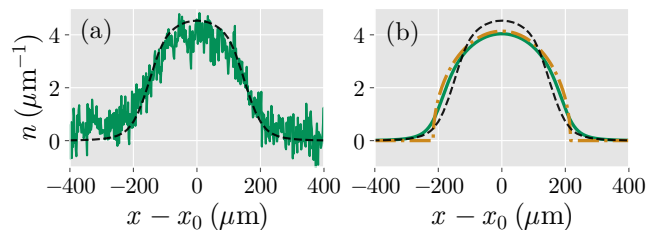


Figure 4. (a) Curves of Fig. 3(c) for the expansion time $\tau = 50$ ms. Solid-line: data; dashed-line: GHD calculations. (b) Comparison of the GHD profile (dashed line) with the profile deduced from the asymptotic formula Eq. 1 (green solid line). Yellow dash-dotted line: asymptotic profile for the half-circle distribution of a zero-temperature quasiBEC of density $n(x_0)$.

We performed such fits using a homogeneous thermal state in the slice, with the temperature as fit parameter. Fitting the expansion for the central slice (Fig. 3-4), we find a temperature $T_{\text{fit}} = 230\text{nK}$, 2.5 times higher than T_{YY} . Although T_{fit} differs strongly from T_{YY} , the rapidity distributions corresponding to these two temperatures are close. This is because, near the quasicondensate regime, the rapidity distribution is dominated

by interaction effects and it only mildly depends on the temperature. Also, we observe that the ratio $T_{\text{fit}}/T_{\text{YY}}$ is maximal for the slice at $x_0 = 0$, and it decreases for slices that are further away from the cloud center.

The spatially-dependent temperatures deduced from the fits with GHD of the expansion profiles are incompatible with the fact the cloud shape is time invariant. The origin of this inconsistency still needs to be elucidated. It might be the signature that the rapidity distribution is non thermal. However more spurious effects cannot be excluded.

Conclusion. We implemented a local probe of the rapidity distribution of our 1D gases, performing a spatial selection followed by a 1D expansion. For a precise analysis of the profiles after expansion, one needs to take into account the finite expansion time, which can be done using GHD calculations, since our expansion indeed follow hydrodynamics. Applied to non-equilibrium scenarios,

this probe of rapidity distribution will be able to reveal the GHD dynamics at play. In particular, in a Newton's cradle setup [18], it should reveal the double peaked local rapidity distribution at the position and time at which clouds collide. In a bipartite quench protocol [28, 44], it should give insight on the peculiar rapidity distribution expected in the merging region. It might also be used to reveal and characterise non thermal stationary states of the Lieb-Liniger model, such as those expected to emerge in the presence of atom losses [60].

Acknowledgment. We thank Marc Cheneau for carefully reading the manuscript, and Sasha Gamayun and Frederik Møller for useful discussions. The authors thanks Dr Sophie Bouchoule, Alan Durnez and Abdelmounaim Harouri of C2N laboratory (UMR 9001, CNRS - UPSACLAY) for the chip fabrication. This work was supported by the Labex Palm projet "Bato" and by ANR Project QUADY-ANR-20-CE30-0017-01.

-
- [1] I. Bloch, J. Dalibard, and W. Zwerger, *Reviews of modern physics* **80**, 885 (2008).
- [2] I. Bloch, J. Dalibard, and S. Nascimbene, *Nature Physics* **8**, 267 (2012).
- [3] B. L. Tolra, K. M. O'Hara, J. H. Huckans, W. D. Phillips, S. L. Rolston, and J. V. Porto, *Phys. Rev. Lett.* **92**, 190401 (2004).
- [4] B. Paredes, A. Widera, V. Murg, O. Mandel, S. Fölling, I. Cirac, G. V. Shlyapnikov, T. W. Hänsch, and I. Bloch, *Nature* **429**, 277 (2004).
- [5] T. Kinoshita, T. Wenger, and D. S. Weiss, *Science* **305**, 1125 (2004).
- [6] T. Kinoshita, T. Wenger, and D. S. Weiss, *Physical review letters* **95**, 190406 (2005).
- [7] H. Moritz, T. Stöferle, K. Günter, M. Köhl, and T. Esslinger, *Physical review letters* **94**, 210401 (2005).
- [8] E. Haller, M. Gustavsson, M. J. Mark, J. G. Danzl, R. Hart, G. Pupillo, and H.-C. Nägerl, *Science* **325**, 1224 (2009).
- [9] Y.-a. Liao, A. S. C. Rittner, T. Paprotta, W. Li, G. B. Partridge, R. G. Hulet, S. K. Baur, and E. J. Mueller, *Nature* **467**, 567 (2010).
- [10] A. Van Amerongen, J. Van Es, P. Wicke, K. Kheruntsyan, and N. Van Druten, *Physical review letters* **100**, 090402 (2008).
- [11] T. Jacqmin, J. Armijo, T. Berrada, K. V. Kheruntsyan, and I. Bouchoule, *Physical review letters* **106**, 230405 (2011).
- [12] X.-W. Guan, M. T. Batchelor, and C. Lee, *Reviews of Modern Physics* **85**, 1633 (2013).
- [13] P. Wicke, S. Whitlock, and N. Van Druten, *arXiv preprint arXiv:1010.4545* (2010).
- [14] G. Pagano, M. Mancini, G. Cappellini, P. Lombardi, F. Schäfer, H. Hu, X.-J. Liu, J. Catani, C. Sias, M. Inguscio, *et al.*, *Nature Physics* **10**, 198 (2014).
- [15] K. V. Kheruntsyan, D. M. Gangardt, P. D. Drummond, and G. V. Shlyapnikov, *Physical Review Letters* **91**, 10.1103/physrevlett.91.040403 (2003).
- [16] A. Vogler, R. Labouvie, F. Stubenrauch, G. Barontini, V. Guarrera, and H. Ott, *Physical Review A* **88**, 031603 (2013).
- [17] B. Fang, A. Johnson, T. Roscilde, and I. Bouchoule, *Physical review letters* **116**, 050402 (2016).
- [18] T. Kinoshita, T. Wenger, and D. S. Weiss, *Nature* **440**, 900 (2006).
- [19] A. Daley, M. Rigol, and D. Weiss, *New Journal of Physics* **16**, 095006 (2014).
- [20] T. Langen, S. Erne, R. Geiger, B. Rauer, T. Schweigler, M. Kuhnert, W. Rohringer, I. E. Mazets, T. Gasenzer, and J. Schmiedmayer, *Science* **348**, 207 (2015).
- [21] M. Schemmer, I. Bouchoule, B. Doyon, and J. Dubail, *Phys. Rev. Lett.* **122**, 090601 (2019).
- [22] J. M. Wilson, N. Malvania, Y. Le, Y. Zhang, M. Rigol, and D. S. Weiss, *Science* **367**, 1461 (2020), publisher: American Association for the Advancement of Science Section: Report.
- [23] W. Kao, K.-Y. Li, K.-Y. Lin, S. Gopalakrishnan, and B. L. Lev, *Science* **371**, 296 (2021).
- [24] V. E. Korepin, N. M. Bogoliubov, and A. G. Izergin, *Quantum inverse scattering method and correlation functions*, Vol. 3 (Cambridge university press, 1997).
- [25] M. Gaudin, *The Bethe Wavefunction* (Cambridge University Press, 2014).
- [26] E. H. Lieb and W. Liniger, *Phys. Rev.* **130**, 1605 (1963).
- [27] E. H. Lieb, *Physical Review* **130**, 1616 (1963).
- [28] B. Bertini, M. Collura, J. De Nardis, and M. Fagotti, *Phys. Rev. Lett.* **117**, 207201 (2016).
- [29] V. B. Bulchandani, R. Vasseur, C. Karrasch, and J. E. Moore, *Physical review B* **97**, 045407 (2018).
- [30] S. Gopalakrishnan, D. A. Huse, V. Khemani, and R. Vasseur, *Physical Review B* **98**, 220303 (2018).
- [31] D. Jukić, R. Pezer, T. Gasenzer, and H. Buljan, *Phys. Rev. A* **78**, 053602 (2008).
- [32] A. Campbell, D. Gangardt, and K. Kheruntsyan, *Phys. Rev. Lett.* **114**, 125302 (2015).
- [33] I. Bouchoule and J. Dubail, *J. Stat. Mech.* **2022**, 014003 (2022).
- [34] N. Malvania, Y. Zhang, Y. Le, J. Dubail, M. Rigol, and D. S. Weiss, *Science* **373**, 1129 (2021).
- [35] K.-Y. Li, Y. Zhang, K. Yang, K.-Y. Lin, S. Gopalakrish-

- nan, M. Rigol, and B. L. Lev, *Physical Review A* **107**, L061302 (2023).
- [36] Y. Le, Y. Zhang, S. Gopalakrishnan, M. Rigol, and D. S. Weiss, *Nature*, 1 (2023).
- [37] V. Dunjko, V. Lorent, and M. Olshanii, *Physical Review Letters* **86**, 5413 (2001).
- [38] M. Rigol, V. Dunjko, and M. Olshanii, *Nature* **452**, 854 (2008).
- [39] J.-S. Caux and R. M. Konik, *Physical review letters* **109**, 175301 (2012).
- [40] F. H. L. Essler, G. Mussardo, and M. Panfil, *Physical Review A* **91**, 051602 (2015).
- [41] L. Vidmar and M. Rigol, *Journal of Statistical Mechanics: Theory and Experiment* **2016**, 064007 (2016).
- [42] F. H. Essler and M. Fagotti, *Journal of Statistical Mechanics: Theory and Experiment* **2016**, 064002 (2016).
- [43] C.-N. Yang and C. P. Yang, *Journal of Mathematical Physics* **10**, 1115 (1969).
- [44] O. A. Castro-Alvaredo, B. Doyon, and T. Yoshimura, *Phys. Rev. X* **6**, 041065 (2016).
- [45] J. De Nardis, B. Doyon, M. Medenjak, and M. Panfil, *Journal of Statistical Mechanics: Theory and Experiment* **2022**, 014002 (2022).
- [46] V. Alba, B. Bertini, M. Fagotti, L. Piroli, and P. Ruggiero, *Journal of Statistical Mechanics: Theory and Experiment* **2021**, 114004 (2021).
- [47] V. B. Bulchandani, S. Gopalakrishnan, and E. Ilievski, *Journal of Statistical Mechanics: Theory and Experiment* **2021**, 084001 (2021).
- [48] A. Bastianello, A. De Luca, and R. Vasseur, *Journal of Statistical Mechanics: Theory and Experiment* **2021**, 114003 (2021).
- [49] A. C. Cubero, T. Yoshimura, and H. Spohn, *Journal of Statistical Mechanics: Theory and Experiment* **2021**, 114002 (2021).
- [50] M. Borsi, B. Pozsgay, and L. Pristvýk, *Journal of Statistical Mechanics: Theory and Experiment* **2021**, 094001 (2021).
- [51] B. Doyon, S. Gopalakrishnan, F. Møller, J. Schmiedmayer, and R. Vasseur, *arXiv preprint arXiv:2311.03438* (2023).
- [52] M. Schemmer, *Out-of-equilibrium dynamics in 1D Bose gases*, phdthesis, Université Paris Saclay (COMUE) (2019).
- [53] T. Jacqmin, J. Armijo, T. Berrada, K. V. Kheruntsyan, and I. Bouchoule, *Phys. Rev. Lett.* **106**, 230405 (2011).
- [54] M. Olshanii, *Physical review letters* **81**, 938 (1998).
- [55] A. Marte, T. Volz, J. Schuster, S. Dürr, G. Rempe, E. G. M. van Kempen, and B. J. Verhaar, *Phys. Rev. Lett.* **89**, 283202 (2002), publisher: American Physical Society.
- [56] B. Doyon, *SciPost Physics Lecture Notes*, 018 (2020).
- [57] B. Doyon, J. Dubail, R. Konik, and T. Yoshimura, *Physical review letters* **119**, 195301 (2017).
- [58] E. Bettelheim, *Journal of Physics A: Mathematical and Theoretical* **53**, 205204 (2020).
- [59] F. Møller, P. Schüttelkopf, J. Schmiedmayer, and S. Erne, *arXiv preprint arXiv:2304.10533* (2023).
- [60] I. Bouchoule and J. Dubail, *Phys. Rev. Lett.* **126**, 160603 (2021), publisher: American Physical Society.